Laser Forming of Complex Structures

Peng Cheng[1], Andrew J. Birnbaum[1], Y. Lawrence Yao[1]
David P. Mika[2], Wenwu Zhang[2], Michael Graham[2], Jud Marte[2], Marshall Jones[2]

[1]Department of Mechanical Engineering, Columbia University, New York, NY, 10027, USA
[2]Global Research Center, General Electric Co., Niskayuna, NY, 12309, USA

Abstract: High-intensity laser beams can be used to heat and bend sheet metal, but the mechanisms of the laser forming (LF) process are not well understood or precisely controllable. The objective of the NIST-sponsored project "Laser Forming of Complex Structures" is to develop technologies for controllable, repeatable laser forming processes that shape and re-shape a wide array of forms and compositions. One such form is embodied in turbomachinery compressor airfoils, characterized by complex 3D geometries and large thickness variation. LF can be used to alter or "tune" the shape of these parts into their final tolerances. To gain insight in applying laser forming to compressor airfoils, LF analysis and process synthesis on tapered-thickness plates is conducted. The bending mechanisms and parametric effects on the deformation characteristics of tapered-thickness plates are investigated. A strategy of LF process synthesis of doubly curved shapes is also presented. The scanning paths are determined by considering the different weights of bending and in-plane strain. A thickness-dependent database is established by LF simulation and experiment, and the heating conditions are determined by matching the ratio of bending strain to in-plane strain between the required values and the laser forming values. The analysis and the synthesis are validated by numerical simulation and experiments. As an example of industrial application, 3D shape tuning of compressor airfoils is also carried out.

1 Introduction

Laser forming (LF) is a non-traditional forming process that does not require hard tooling or external forces and hence, dramatically increases process flexibility and can reduce the cost of forming processes. It has great promise to become an inexpensive and flexible mainstream manufacturing process for both rapid prototyping and manufacturing applications. A typical application might call for small secondary deformations for shape tuning or distortion correction of formed, machined or welded components [1]. Compressor airfoil shape tuning by LF is one of the objectives in the NIST-sponsored project "Laser Forming of Complex Structures." To implement LF in the shape tuning of compressor airfoils, complex 3D geometries with large thickness and curvature change, the analysis and process synthesis of tapered-thickness plate LF is initiated to improve the understanding and application of 3D laser forming.

Numerous investigations of laser forming processes have been carried out to elucidate process mechanisms and effects of key process parameters on both dimension and mechanical properties [2,3,4]. We term this type of analyses *forward-type:*

$$f\left(X^0, Y^0, Q^0 \text{ power, spot size, velocity, etc.}\right) = X^1, Y^1, Q^1 \qquad (1)$$

where X^0 and X^1 are the initial and final geometric configuration, respectively, and Y^1, Q^1 are respectively the resulting microstructure and properties. Geometric effects, especially due to thickness, play an important role in laser forming. For example, Vollertsen [5] proposed a simple two-layer model based on the temperature gradient mechanism (TGM) and reported bending inversely proportional to the

square of the plate thickness. Another analytic model has been introduced to capture the effects of changing sheet width and length dimensions [6]. In general researchers have focused on constant thickness cases, so more generalized models are required for 3D shape analysis.

In addition, for laser forming to become industrially useful, robust process synthesis must be improved. Process synthesis is the design of process parameters (laser scanning paths and heating conditions) required to obtain a desired shape, microstructure and properties. We term this type of analyses *inverse-type:*

$$g\left(X^0, X^1, Y^0, Y^1, Q^0, Q^1\right) = \text{power, spot size, velocity, etc.} \tag{2}$$

A thorough understanding of forward type problems is required for inverse analysis. In recent years, inverse methodology has been improved from simple empirical methods to more physics-based methods. For example, Edwardson *et al.* [7] proposed that scan paths should be perpendicular to curvature gradients in constant thickness doubly curved shapes. Cheng and Yao [8] proposed LF strategies for very thin plate based on in-plane strains generated by finite element methods (FEM). Liu and Yao [9] developed similar strategies for thicker plate by considering both in-plane and bending strains. As is the case in forward-type analysis research, proposed methods have been concerned only with uniform thickness plate, neglecting the effects of thickness on bending strain, which can have a significant contribution.

In the present paper, experiment and simulation of laser forming on tapered-thickness plate and compressor airfoils is reported. Temperature field and bending deformation under straight-line scanning on tapered-thickness plate is investigated as well as parametric effects such as scanning speed and beam spot size on bending deformation. We propose a strategy for the inverse analysis of doubly curved shapes with varying thickness. The strategy utilizes FEM to generate a deformation map from the initial to final configurations, and heating paths are determined by weighted-averages of the minimum principal in-plane and bending strains. In addition, a thickness-dependent database is established by experiment and FEM to determine heating conditions. An example of compressor airfoil shape tuning by LF is also presented.

The goal of this template is to achieve uniformity in the paper. The typography, layout and style used in these instructions are exactly the same, as you should use when preparing your paper. Please use this template and simply overwrite the text. If you copy and paste text into the template then it will retain the style from the original, hence you must reapply the appropriate style for the proceedings.

2 Forward-Type Process Analysis

2.1 Experiments and Simulation

Figure 1 shows the compressor airfoil geometry and the tapered-thickness plate. The airfoil is composed of wrought polycrystalline alloy 718 extruded and formed into the present shape. Alloy 718 is a nickel-based superalloy widely used in aircraft turbomachinery applications [10]. The airfoil is approximately 50 mm in length with thickness continuously varying from approx 0.6-mm at the leading and trailing edges to 2.5-mm at the center. The plate was cut from 3.0-mm AISI 1010 rolled-stock steel sheet with one surface machined to result in a linearly tapered thickness in one direction from 1 mm at two opposite edges to 3-mm at the corresponding centerline; the thickness is constant in orthogonal plate directions, and the width and length are 80-mm. The plate geometry was chosen to isolate the effects of thickness deviation without inducing other complexities and at the same time without loss of the generality. The

applied laser system for tapered plate is a PRC-1500 CO_2 laser with maximum output of 1.5 kW operating in a continuous wave (CW) mode with beam power density following a Gaussian function (TEM_{00}). The irradiated plate surface is coated with graphite to enhance the absorption of heat input. A 2kW max output Nd:YAG laser was used in concert with a 6-axis robot in a part-carry mode for airfoil tuning. No coatings were used on the airfoil, however, sufficient argon gas coverage is required to prevent undesirable oxidation.

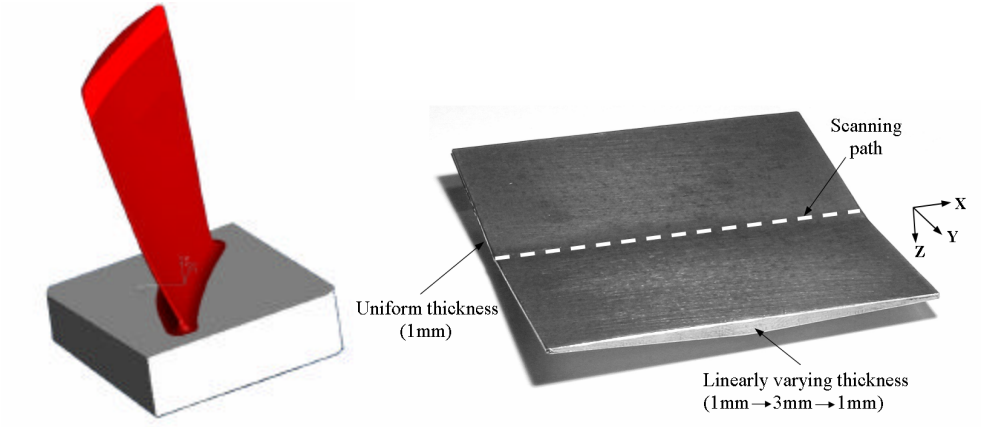

a) Airfoil geometry b) AISI 1010 double-tapered plate

Figure 1: Part geometries: a) Compressor airfoil. b) Tapered AISI 1010 plate shown post LF under a 1000 W, 20 mm/s, 8 mm beam spot size and 10 times scan

Details of simulation methodology are described in an earlier paper [4]. In the simulations, material properties such as the modulus of elasticity, heat transfer, thermal conductivity, specific heat, and flow stress are all considered temperature dependent. A strain-hardening coefficient, which is also temperature dependent, is defined in order to capture strain hardening of the material. No melting is involved in the forming process.

2.1.1 Alloy 718 Processing

Because airfoil shape tuning is carried out on near net shape parts, disturbances in the microstructure that may degrade properties critical to performance such as tensile strength, hardness, or fatigue life must be avoided. The challenge is to find tempered lasing parameters that meet these requirements while providing a rich dataset that can produce the required level of strains. For example, lasing that melts or recrystallizes the underlying microstructure must be avoided (See Figure 2). However turbo machinery applications of 718 rely on strengthening mechanisms that degrade before recrystallization takes place.

The 718 alloy is typically used in the solution treated and precipitation hardened condition (See Figure 3). The microstructure consists of an austenitic solid solution of Ni-Fe-Cr, with niobium rich carbides, laves phase (Ni_2Nb), and δ (Ni_3Nb), γ'(Ni_3(Al, Ti, Nb, V)), and γ''(Ni_3(Nb, Ti)) precipitates. The most potent strengthener in 718 is the γ'' precipitate which usually occurs as disk-shaped particles less than 60 nm in diameter and 10 nm thick [11]. Because of its size γ'' is directly detected by TEM techniques, but because the present study seeks to test a large number of samples, this option is cost prohibitive. The presence of γ'' can however be inferred economically by microhardness measurements, with HRC 40-45 being a positive indicator of γ'' [11].

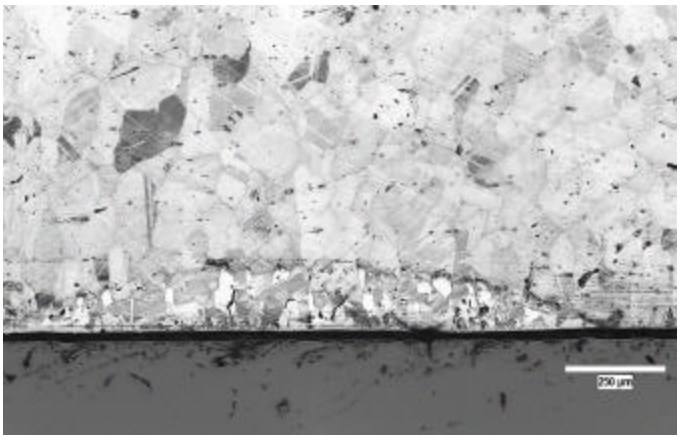

Figure 2: Optical micrograph of 718 recrystallization caused by high-temperature laser forming

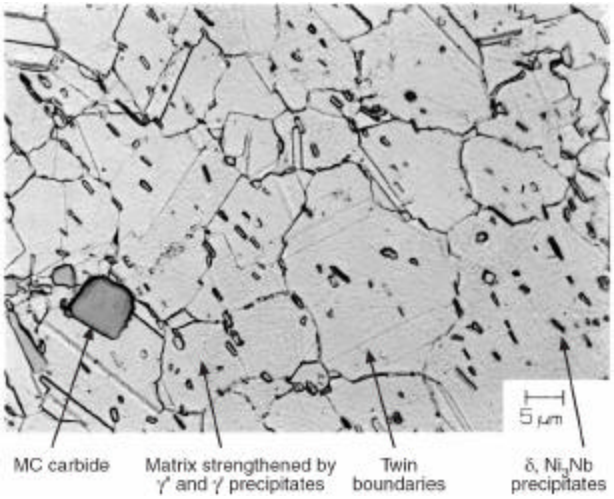

Figure 3: A typical microstructure for solution treated and precipitation hardened alloy 718

An experimental matrix was designed to map lasing parameters to both geometry and microstructural outcome. Rectangular flat coupons wire-EDM cut from rolled 718 with dimensions close to the size of the airfoil were used: 0.625, 1.60 and 2.50-mm thick by 55.0 x 25.0-mm. The coupons were solution treated and precipitation hardened and subsequently tumbled in an abrasive media to replicate as much as possible the microstructure and surface characteristics of the airfoil. All testing was done under argon coverage to avoid oxidation and no coatings were employed to enhance laser energy absorption. Several parallel straight line scans were performed on each coupon while temperatures were recorded with a two-color pyrometer; resulting bending was determined by an optical profilometer.

2.2 Results and Discussions

2.2.1 Deformation Characteristics

Figure 4 shows the bending angle of a tapered and 2-mm uniform thickness plate under LF conditions of P=1000W, V=20mm/s and spot size=8mm. Compared with the uniform thickness plate, the tapered plate has a significant bending angle variation along the scan line. This nonuniformity can be attributed

to two main factors: varying bending rigidity and temperature field along the scan. Fig.5 shows a comparison of peak temperature distribution between tapered and uniform thickness plates for both the scanned and opposite (unscanned) surfaces. For both cases, the peak temperature is lower at the entrance and higher at the exit of the scanning path due to the edge effect [12]. For the uniform thickness plate, as expected, the peak temperature is constant along the scanning path excepting the two ends. For the tapered-thickness plate, the peak temperature on both scanned and unscanned surfaces decreases with increasing thickness. The decrease is due to the increasing heat sink brought about by the increasing plate thickness. Since the peak temperature decrease on the unscanned surface is much larger than that of the scanned surface, the temperature gradient through the thickness direction increases with the increasing plate thickness.

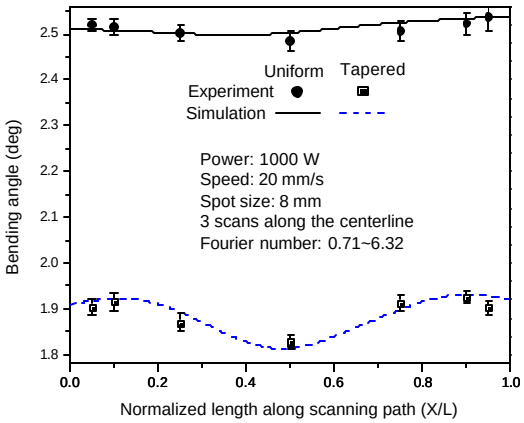

Figure 4: Bending angle variation along the scanning direction for both 1-3-1-mm tapered thickness and 2-mm uniform thickness plates

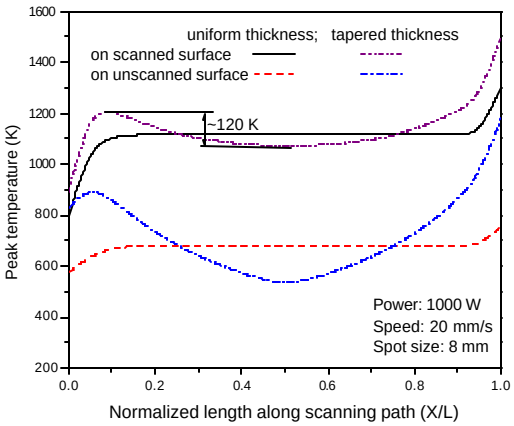

Figure 5: Comparison of the temperature distribution along the scanning path between 1-3-1-mm tapered thickness and 2-mm uniform thickness plates

From the bending variation shown in Figure 4, it is also seen that the bending angle increases first then decreases from the ends to the center of the scanning line. There are two competing mechanisms that affect bending along the line: there exists an increasing temperature gradient through the thickness from the ends to the center to increase bending, and there is higher bending rigidity at the center due to increased thickness that will decrease bending. As the thickness increases, the effect of bending rigidity in this case begins to dominate to cause the bending angle to decrease. A more quantitative estimation of the dominant bending mechanism can be had via the modified Fourier number.

The modified Fourier number $F_0 = a \cdot d /(h^2 \cdot v)$, where $a, d, h,$ and v are thermal diffusivity, beam diameter at workpiece surface, sheet thickness and scanning speed, respectively, has been used to approximately estimate the laser forming mechanism [3]. In the present case of study, F_0 varies from 6.3 to 0.7 as the thickness varies from 1 mm to 3 mm, indicating a likely mechanism transition along the scanning line from the upset mechanism (UM) in thin regions to TGM in thicker regions. The temperature distribution (Figure 5) indicates there are no steep through-thickness temperature gradients and there exists much more thickness-direction plastic strain in thinner regions, both hallmarks of UM (See Figure 16). In contrast, thick regions have higher through-thickness temperature gradients and lower through-thickness strain, defining characteristics of TGM.

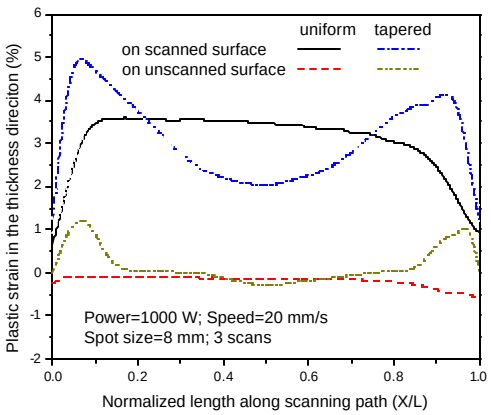

Figure 6: The distribution of plastic strain in Z direction along the scanning path

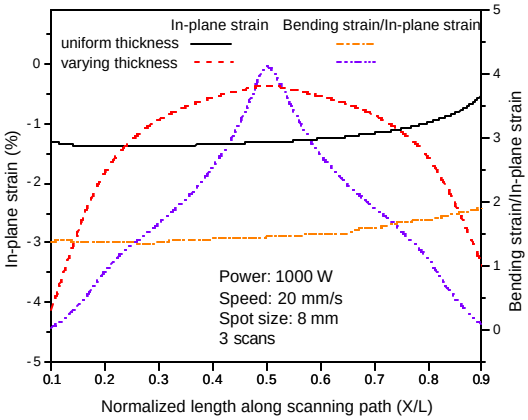

Figure 7 Distribution of in-plane strain and strain ratio calculated on top surface (z=h/2)

Applying continuum deformation theory to our deformed plates, the strain field can be locally projected to planes at the mid and outer surfaces to consider in-plane strain that expands and/or contracts the surfaces. Further, this in-plane strain can be decomposed into principal components and corresponding directions. In any given direction, the strain difference between the scanned and mid surfaces can be considered and is directly related to bending strain that bends the plate towards the scanned surface. Figure 7 shows the distribution of in-plane strain and the ratio of bending strain to in-plane strain (calculated on top surface) for uniform and varying thickness plate. It is seen that the strain ratio increases with the thickness, which means the effect of bending strain plays more important role in bending the thicker regions of the plate. This is consistent with the previous analysis that TGM is dominant in the thicker regions.

2.2.2 Parametric Study

Referring to Figure 8, when the scanning speed changes, a number of effects combine to influence bend angle and its variation with thickness. In general, the average bending angle decreases with increasing scanning speed due to a decrease in effective heat input, so that both the peak temperature and temperature gradient through the thickness decrease. In addition, bending variations along the scan decrease with increasing scanning speeds because temperature gradients between thicker and thinner locations also decrease with scanning speed. It is also noted that with increasing speed, the Fourier number varies less along the scan and the laser forming mechanism is more consistently TGM. As a result, faster scanning speeds help to achieve more uniform bending deformations in the tapered plate.

When the beam spot size increases, the deformation uniformity decreases along with the average bending deformation. The reason is because both the peak temperature and through-thickness temperature gradient decrease with increasing beam spot size, but the temperature gradient in the thicker regions decreases much more than that of the thinner regions. For the thicker regions where the laser forming mechanism is primarily in TGM, the larger drop in temperature gradient reduces the bending deformation much more than in thinner regions. Since the bending deformation in thicker regions is already smaller than that of the thinner region due to the larger bending rigidity, the variations of bending deformation will increase with beam spot size.

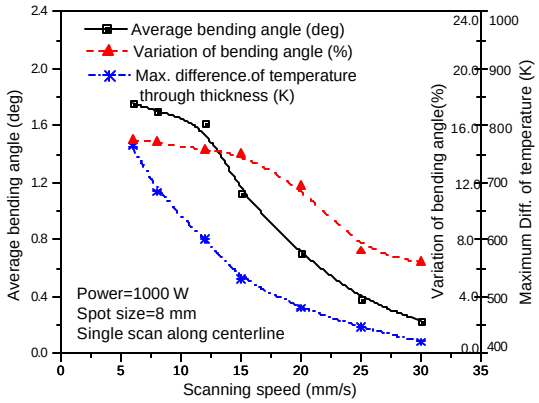

Figure 8: Bending angle and angle variation with various scanning speeds on tapered plate (Power=1000 W, spot size=8 mm, single scan along the centerline)

3 Inverse-Type Process Synthesis

The process design of laser forming on varying thickness plate differs from the process applied on uniform thickness plate. Not only must shape curvature be considered, but also thickness variations in determining the scanning path. The strain or strain ratio is a function of power, scanning velocity, beam spot size, and thickness. In tapered thickness plate, even under constant heating conditions (laser power, scanning velocity and beam spot size) the bending mechanism may vary along the scanning path, as shown above.

An overall strategy for process design of laser forming on tapered thickness plates is presented in Figure 9 and involves three steps. The first step is to determine a compatible strain field that maps the initial configuration to the desired configuration. This is done in many cases most easily using FEM with judicious application of boundary conditions to find the deformation mapping using *linearly elastic* material response. The resulting strain fields can then be projected and decomposed it into in-plane and bending strain components at both mid and outer surfaces. The second step is to determine the scanning paths by locating paths perpendicular to weighted average-strain directions, to be described below. The weighting is chosen to emphasize bending strain in thicker locations where TGM is dominant, but shape curvature is considered as well. The third step is to determine heating conditions from the thickness-dependent databases established by laser forming simulation and experiment. By matching the strain and strain ratio between the required values and those of the database, the laser power and scanning speed can be determined if the beam spot size is assumed constant.

The experiment and simulation for the inverse analysis was carried out on a second plate geometry, which also is tapered from 1-mm to 3-mm to 1-mm as before, but in a quadratic fashion instead of linearly as previously described. The material and fabrication methods are the same as previously described. We employ a coordinate system at one corner of the plate such that the tapered thickness direction corresponds to the y-direction and the thickness direction is the z-direction. This describes the initial configuration. The desired configuration is a pillow shape and is given in terms of the middle surface, $S(x,y)$, (the surface midway between top and bottom surfaces) as follows: $S(x,y)=A(x)+B(y)$, where $A(x)$ and $B(y)$ are cubic-spline functions, $x, y \in [-40,40]$, such that $B(y)$ is defined by the three nodes {(-40, -40, 0), (-40, 0, 3.5), (-40, 40, 0)} and $A(x)$ is defined by {(-40, 0, 0), (0, 0, 5), (40, 0, 0)}.

Thus, the pillow configuration is doubly-curved. The quadratic-tapered plate in the final configuration is shown in Figure 10.

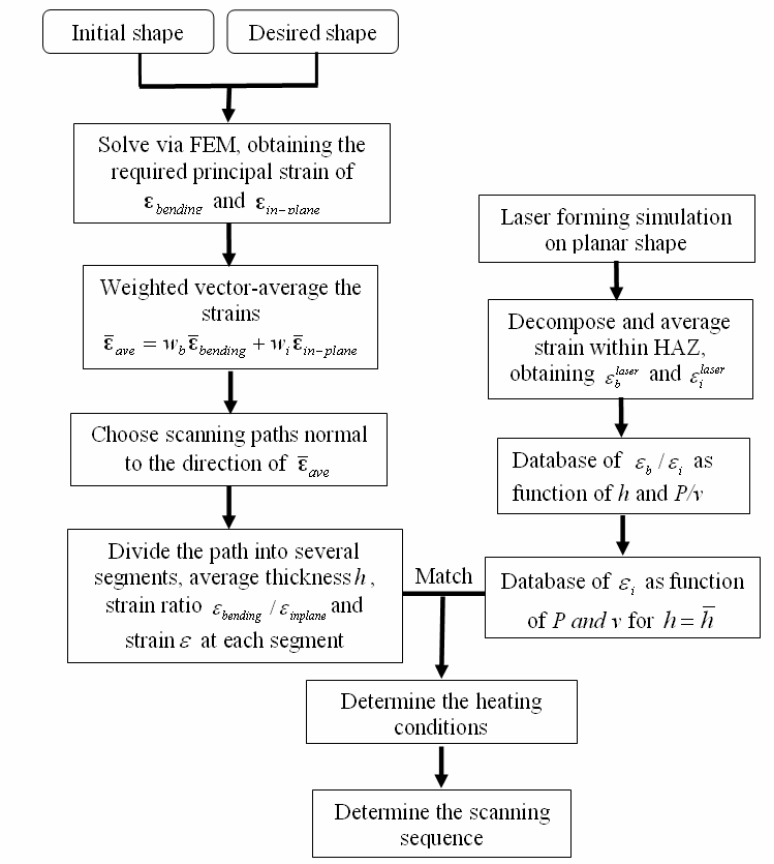

Figure 9: Flow chart of laser forming process design for varying thickness shape

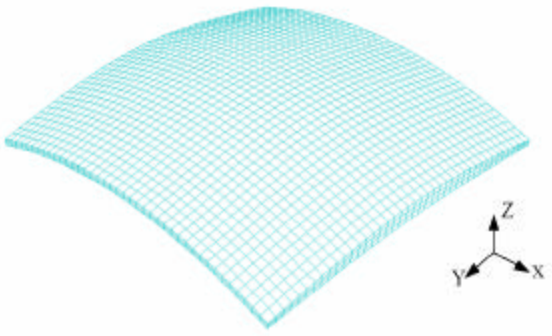

Figure 10: Quadratic tapered plate in the final pillow-shaped configuration. The quadratic taper is in the y-direction from 1-mm at the edges to 3-mm at the center; the thickness is constant in the x-direction

3.1 Scanning Path Determination

As described above, the required strain field is obtained by constraining the initial shape to the final shape in a large-deformation linearly elastic FEM model. The total strains in a layer of the plate parallel and a distance *z* from the middle surface can be decomposed as

$$
\begin{aligned}
e_{xx} &= e^{I}_{xx} - z\frac{\partial^2 w_0}{\partial x^2} = e^{I}_{xx} + e^{B}_{xx} \\
e_{yy} &= e^{I}_{yy} - z\frac{\partial^2 w_0}{\partial y^2} = e^{I}_{yy} + e^{B}_{yy} \\
e_{xy} &= e^{I}_{xy} - z\frac{\partial^2 w_0}{\partial x \partial y} = e^{I}_{xy} + e^{B}_{xy}
\end{aligned}
\tag{3}
$$

where e^{I} is strain in the middle surface and e^{B} is the bending strain. We note that bending strain is a product of curvature and distance from the middle surface, whereas in-plane strain is uniform through the thickness.

Figure 11 shows principal strain directions for both in-plane and bending strain components of the quadratic-tapered plate in the final pillow-shaped configuration. An examination of the figure shows that the in-plane strain magnitude (calculated at plane z=0) does not change with thickness, but the bending strain increases in Y-direction with thickness. Laser forming generally produces both in-plane and bending strains with the dominant strain occurring perpendicular to the scanning path. Since the influence of bending strain and in-plane strain varies with thickness and curvature, as seen in the case considered, it is appropriate in determining scanning paths to vector average the principal in-plane strain and principal bending strain directions.

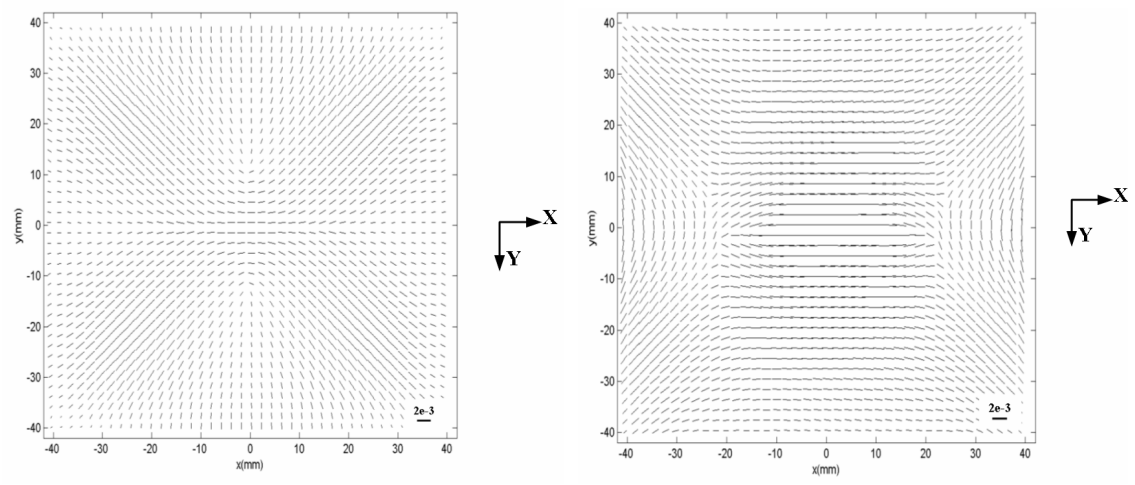

Figure 11: Principal strain direction plots of the quadratic-tapered plate in the pillow-shaped configuration: (a) in-plane strain, and (b) bending strain

Ueda [13,14,15] investigated the relation between in-plane strain and bending strain and pointed out that bending strain is proportional to the product of thickness and curvature and in-plane strain is proportional to the square of curvature. Therefore, the ratio of bending strain to in-plane strain can be expressed as

$$e_B / e_I \propto t / r \tag{4}$$

where t is the thickness and r the curvature. The above relation illustrates that the relative effect of bending strain over in-plane strain increases with increasing thickness, and the relative effect of in-plane over bending strain increases with curvature. The employed weighting scheme is chosen to capture this effect:

$$\bar{\mathbf{e}}_{ave} = w_B \cdot \mathbf{e}_B + w_I \cdot \mathbf{e}_I = \left[1 + \frac{(t - \bar{t})}{\bar{t}} \frac{\bar{r}}{r}\right] \cdot \mathbf{e}_B + \left[1 - \frac{(t - \bar{t})}{\bar{t}} \frac{\bar{r}}{r}\right] \cdot \mathbf{e}_I \tag{5}$$

where $\mathbf{e}_B$ and $\mathbf{e}_I$ are principal bending and in-plane strains, respectively. t and $\bar{t}$ are local thickness and average thickness, respectively. r and $\bar{r}$ are the absolute value of local Gaussian curvature and average Gaussian curvature of the whole plate, respectively. For a uniform thickness shape, the weight numbers equal unity and the above equation turns to be a commonly used vector averaging method. Figure 12 shows the above weighted average principal strain and resulting chosen paths to deform the quadratic-tapered plate into the pillow shape. It should be noted that the initial path spacing is approximately the width of the plastic deformed zone, which can be assumed to be the beam spot size. Also to note in Figure 12 is that the rule to have paths follow orthogonal to the principal strain field is not strictly enforced. Towards the centerlines there is deviation from the rule to avoid asymptotic paths and practical constrains of the laser system and the current planning algorithm. The deviation is assumed trivial since the strain is small and the determined heating conditions there are also small.

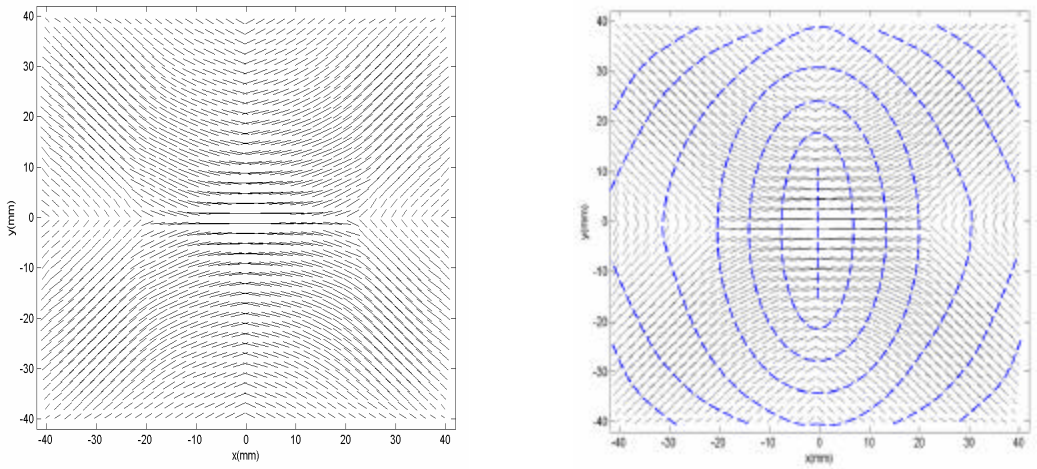

a) b)

Figure 12: a) Vector plot of the averaged in-plane strain and bending strain of the pillow shape, b) the determined heating paths

3.2 Heating Condition Determination

After determination of the scanning paths, the heating conditions including laser power, laser scanning speed, and beam spot size are to be determined. While it is possible to continuously vary each to generate the strain field required to form the desired shape, this study adopts the strategy of constant power and piecewise constant speed for a given path to satisfy the constraints of the current laboratory equipment. A path is broken down to a few segments such that within each segment, the range of total strain variation is about the same as in other segments. Since the thickness varies through the segments, an averaged segment thickness is adopted so that each segment has an equivalent constant thickness.

The in-plane or bending minimal principal strains are first averaged within each segment along a scanning path and lumped between adjacent paths because all these strains are to be imparted by the paths. Within a scanning path, the segment with the largest strain, which has the strongest influence on the final shape, is first chosen. From the AISI 1010 database generated from FEM simulation, strain ratio as a function of thickness and line energy (P/V) is known (Figure 13a), and the line energy can be determined for this segment. The database also can relate in-plane strain as a function of power and velocity for an equivalent thickness (Figure 13b) allowing a combination of power and velocity to be determined. The combination of power and velocity that fulfills the requirement of line energy is the proper heating condition. The determined P value is also adopted for the entire path. For other segments in this path, since the power has been determined, the corresponding scanning velocity can be determined from the database of strain ratio as a function of thickness and line energy. There might be a discrepancy of the strain magnitude between the required values and the laser forming values for those segments except for the first determined one. The reason is because the heating conditions for those segments are only determined by strain ratio and corresponding line energy. Deviations caused by residual discrepancies can be eliminated with iterative laser forming.

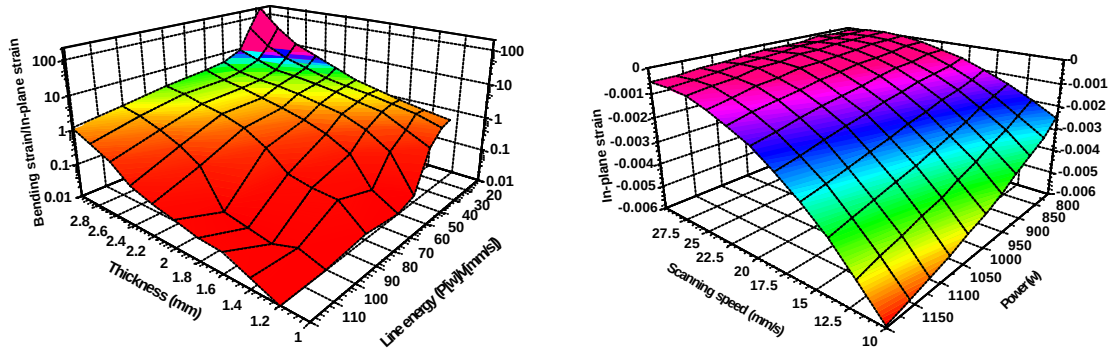

a) b)

Figure 13: Database for the determination of heating conditions a) the ratio of bending strain to in-plane strain as the function of line energy (P/V) and thickness, and b) the in-plane strain for a typical thickness (h=2 mm) as the function of power and scanning speed

Figure 14 shows the formed pillow shape and the deviations under these conditions, respectively. A general agreement can be seen from the figures. Possible sources contributing to the discrepancy include the lumped method used to sum strains between adjacent paths; finite number of paths to approximate a continuous strain field; and constant power within each path and constant velocity within each segment.

3.3 Effective path spacing

The above procedure outlines the determination of paths and heating conditions as discrete activities. We note here that such a serial scheme is not always feasible due to, for example, a narrow processing window caused by microstructural sensitivities such as seen with alloy 718. Similar restrictions can be placed on heating conditions and trajectories due to limitations of the lasing system, such as actuator velocity or acceleration limits, the latency and synchronization of shuttering systems, etc.

It is likely that these limitations can be overcome by the simultaneous rather than discrete determination of scanning paths and heating conditions. To illustrate this, we introduce a new parameter, L, the path

spacing. Now, suppose that a given path spacing L is specified over a region of interest requiring curvature change r. The microstructural and geometric database may indicate that to achieve the desired curvature on the given paths, a very aggressive heating schedule is required– one that has a high probability of microstructural damage. More propitious heating conditions may be found by altering the path spacing and re-querying the database for probable outcome. Thus, the possibility may exist to achieve the desired curvature under more favorable conditions afforded by lower (or maybe even higher) path spacing, L. The manipulation of path spacing can also be used to optimize other aspects of interest such as to minimize bending angle variance. Maximum flexibility is afforded by simultaneously calculating path spacing, path trajectories and heating conditions to accommodate the various microstructural and system constraints.

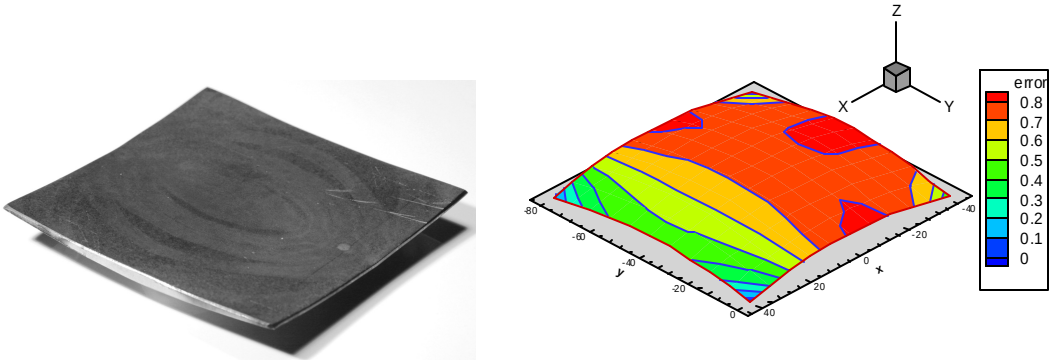

a) b)

Figure 14: a) Formed pillow shape b) deviations between formed shape and desired shape(unit: mm)

4 Airfoil Shape Tuning by Laser Forming

Airfoil shape tuning is a specialized application of laser forming [1]. Compressor airfoils are complex 3D geometries with large thickness variation including very thin leading and trailing edges that can be rapidly heated and damaged. The varying airfoil cross-section in combination with airfoil bow, warpage and twist results in complex 3D structural stiffness. The geometric deviations between as-forged and desired shapes can be eliminated by laser forming if the process can be more robust, quicker and cheaper than alternative shape tuning methods and if LF doesn't reduce material strength, fatigue resistance, material homogeneity or other desirable characteristic.

Figure 15 shows the general strategy and laboratory arrangement for airfoil shape tuning. Given an actual shape, the deviation of one of the airfoil surfaces to the nominal CAD-designed shape can be obtained by optical scanner. The measurement and fitting methods are accurate to approximately +/- 0.025mm. Then the required strain field and the heating paths can be determined following the methods discussed in the previous sections. If the deviation cannot be eliminated by one pass, an iterative approach can be applied utilizing the error between the current and desired shape to give a new scan strategy.

As laser forming of complex structures involves both the forward and inverse type problems, a number of forward-type simulations have been conducted on the airfoil. Figure 16 shows airfoil deformation and temperature fields along with thickness variation under a straight line scan. Consistent with the discussion in the previous sections, bending strain and in-plane strain vary with cross-section thickness, and larger temperature gradients occur at the center of the blade where thickness is the greatest.

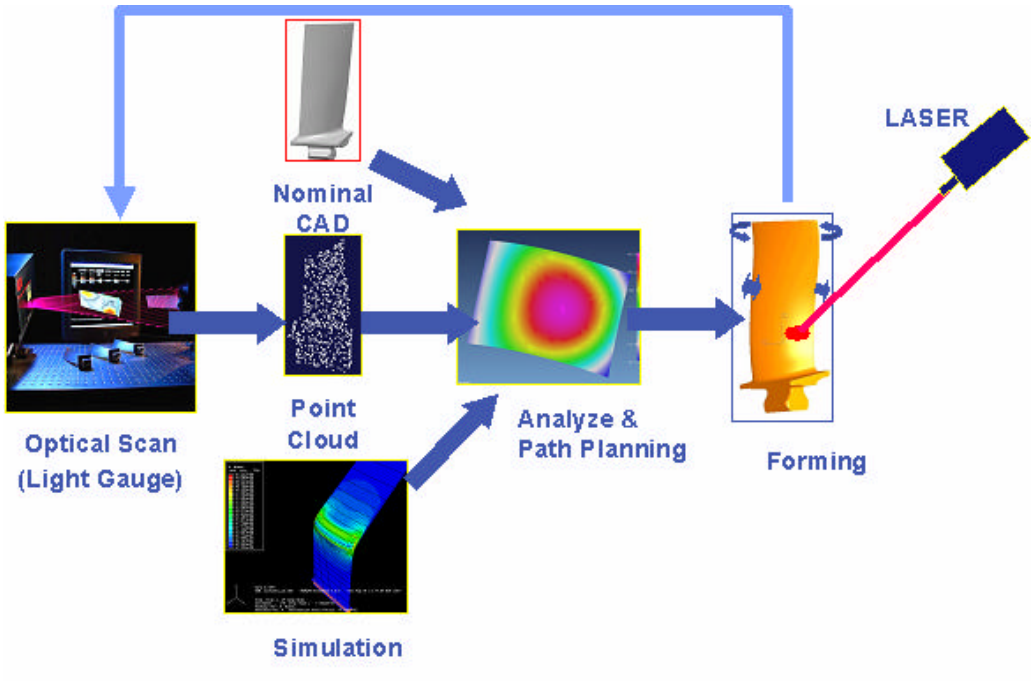

Figure 15: General Strategy for Blade Shape Tuning

Curved scanning paths have also been modeled and compared with experimental results. Due to shape complexity the airfoil LF deformation includes bending, shrinkage, warping and twisting. Compared with experimental results (Figure 17), the forward-type numerical model has shown capable to simulate all the deformation characteristics.

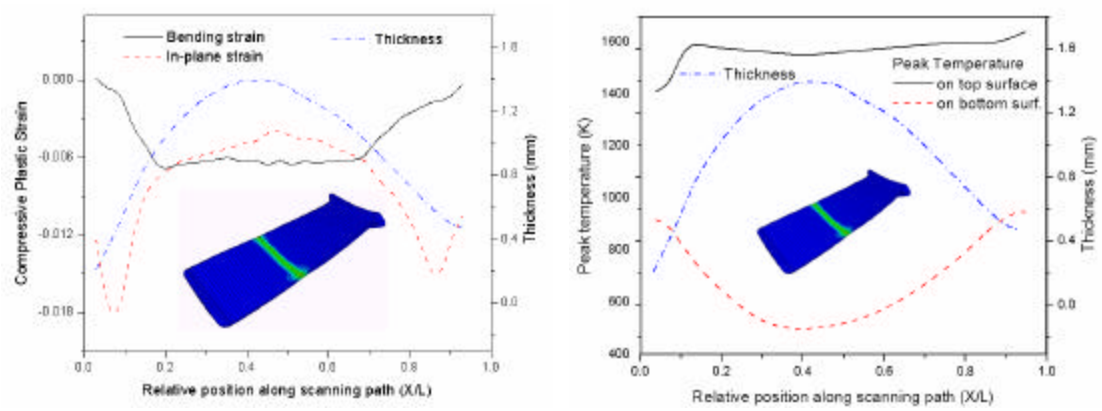

a) b)

Figure 16: a) Distribution of plastic strain, and b) peak temperature along the scanning path (straight line scanning, p=700W, v=150mm/s, spot size=4mm). Note, thickness along the scan is also shown

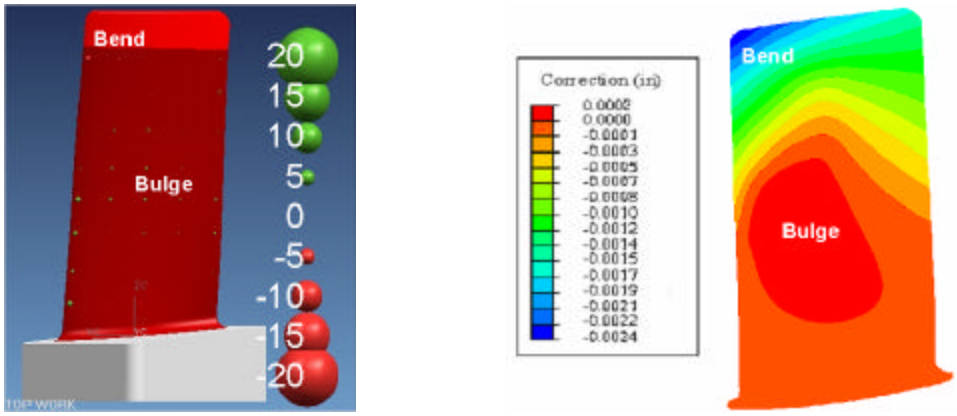

a) b)

Figure 17: Comparison of experimental a) and numerical b) result when scanned along 6 curve lines

With deviations to the desired shape as input, the required strain field can be obtained and decomposed into in-plane and bending strain components; the scanning paths and corresponding heating conditions are designed interactively in the developed LF process design program (shown in Figure 18), following the strategies proposed in the previous sections. Figure 19 shows the simulated tuning result compared with the required values. The deformation trend is agreeable in most of the regions of the airfoil. The discrepancy can be reduced by iterative scans.

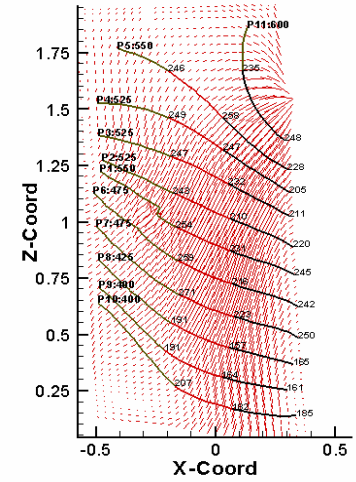

Figure 18: Determined scanning paths, generated by the *Automation System of Process Design for Laser Forming*

5 Conclusions

In order to apply laser forming to the complex structures such as compressor airfoils with large variations of thickness and curvature, the analysis and process synthesis of LF tapered-thickness plate are conducted in this paper. For the process analysis, the deformation nonuniformity is primarily due to the variation of heat sink and the bending rigidity. With increasing thickness, temperature gradient mechanism (TGM) dominates and the bending strain plays a more important role than in-plane strain. Higher scanning speeds and smaller beam spot sizes tend to decrease bending variation along scans.

For the inverse analysis of thin tapered plates, the scanning paths are located perpendicular to the directions obtained by weighted averaging the principal minimum in-plane and bending strains. The weighted vector-averaging method is capable of describing the variation of bending strain effect with the thickness. In determining heating conditions, a database of the strain ratio as a function of laser power, scanning speed and the plate thickness is established. The presented methodology was applied in the compressor airfoil shape tuning. Although there are many practical issues to be solved, laser forming has proven to be a promising technology for industrial applications.

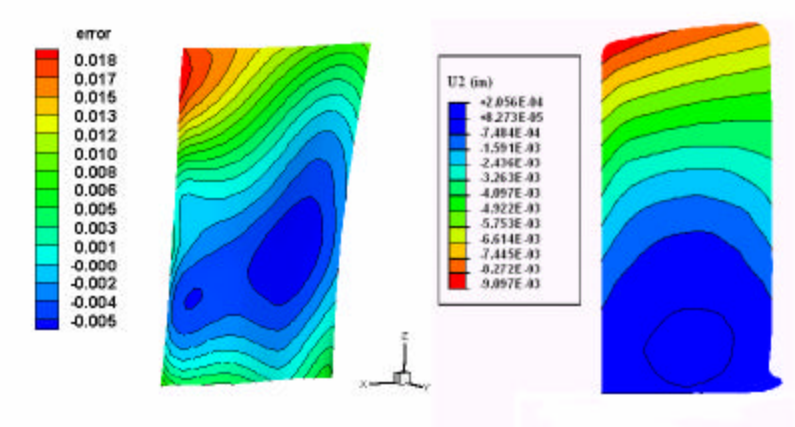

Figure 19: Errors to be removed (left) and the removed errors by LF with designed paths and heating conditions (right) (both with the units of inch)

Acknowledgement

The authors acknowledge the support of the NIST and of co-workers within the NIST-sponsored project "Laser Forming of Complex Structures" (grant number ATP-00005269).

References

1. Wenwu Zhang, Judson Marte, David Mika, Michael Graham, Brian Farrell and Marshall Jones, "Laser Forming: Industrial Applications," *Proceedings of ICALEO 2004*, Section D. pp.27-35.
2. Sprenger, A., Vollertsen, F., Steen, W. F., and Watkins, K., 1994, "Influence of Strain Hardening on Laser Bending," *Laser Assisted Net Shape Engineering, Proceedings of the LANE'94,* Meisenbach, B. eds., Germany**, 1**, pp. 361-370.
3. Li., W., and Yao, Y. L., 2000, "Numerical and Experimental Study of Strain Rate Effects in Laser Forming," ASME J. Manuf. Sci. Eng., **122**, pp. 445-451.
4. Cheng, P., and Yao, Y. L., 2003, "The Influence of Sheet Metal Anisotropy on Laser Forming Process," *Proceedings of the ICALEO'03*, Section E, pp. 1-10.
5. Vollertsen, F., 1994, "An Analytical Model for Laser Bending," Lasers in Engineering, **2**, pp. 261-276.
6. Cheng, P., Yao, Y. L., Liu, C., Pratt, D., and Fan, Y., 2004, "Analysis and Prediction of Size Effect on Laser Forming of Sheet Metal," Transactions of NAMRI/SME, **32**, pp. 439-446.
7. Edwardson, S. P., Moore, A. J., Abed, E., McBride, R., French, P., Hand, D. P., Dearden, G., Jones, J. D. C., and Watkins, K. G., 2004, " Iterative 3D Laser Forming of Continuous Surfaces," *Proceedings of ICALEO 2004*, Section D. pp.36-45.

8. Cheng, J. and Yao, Y. L., 2004, "Process design of laser forming for three-dimensional thin plates," ASME Transactions J. Manu. Science and Engineering, **126**, pp. 217-225.

9. Liu, C., and Yao, Y. L., 2003, "FEM Based Process Design for Laser Forming of Doubly Curved Shapes," ASME Transactions J. Manu. Science and Engineering, submitted.

10. R.E. Schafrik, D.D. Ward, J.R. Groh, 2001, "Application of Alloy 718 in GE Aircraft Engines: Past, Present and Next Five Years", *Proceedings of the International Symposium on Superalloys 718, 625, 706 and Various Derivatives*, pp 1-11. June 17-20. TMS.

11. Liu, L., Hirose, A., and Kobayashi, K. F., 2002, "A numerical approach for predicting laser surface annealing process of Inconel 718," Acta Mat. **50**, pp. 1331-1347.

12. Bao, J., and Yao, Y. L., 2001, "Analysis and Prediction of Edge Effects in Laser Bending," ASME J. Manuf. Sci. Eng., **123**, pp. 53-61.

13. Ueda, K., et al., 1994a, "Development of Computer-Aided Process Planning System for Plate Bending by Line Heating (Report I)-Relation Between Final Form of Plate and Inherent Strain", Journal of Ship Production, **10**(1), pp. 59-67.

14. Ueda, K., et al., 1994b, "Development of Computer-Aided Process Planning System for Plate Bending by Line Heating (Report II)-Practice for Plate Bending in Shipyard Viewed from Aspect of Inherent Strain", Journal of Ship Production, **10**(4), pp. 239-247.

15. Ueda, K., et al., 1994c, "Development of Computer-Aided Process Planning System for Plate Bending by Line Heating (Report III)-Relation Between Heating Condition and Deformation", Journal of Ship Production, **10**(4), pp. 248-257.